Catalysis Today 176 (2011) 318–323

Contents lists available at ScienceDirect

Catalysis Today

journal homepage: www.elsevier.com/locate/cattod

The effect of zirconia and niobia supports on the catalytic activity of surface VO_x species in total oxidation of model volatile organic compounds

A. Adamski [a,*], P. Zapała [a], L. Chmielarz [a], J.A.J. Rodriguez [b], G. Djéga-Mariadassou [c], Z. Sojka [a]

[a] Jagiellonian University, Faculty of Chemistry, Ingardena 3, 30-060 Cracow, Poland
[b] National Institute for Space Research, Combustion and Propulsion Laboratory, Rodovina Presidente Dutra km 40, Cachoeira Paulista, CEP 12630-000, São Paulo, Brazil
[c] Centre of Polymer and Carbon Materials (CMPW) PAS, Curie-Skłodowskiej 34, 41-800 Zabrze, Poland

ARTICLE INFO

Article history:
Received 30 September 2010
Received in revised form
23 November 2010
Accepted 29 November 2010
Available online 30 December 2010

Keywords:
VOC
Total oxidation
Vanadia
ZrO_2
Nb_2O_5
EPR

ABSTRACT

Samples of the catalysts containing 0.5, 5.0 and 40 mol.% of V_2O_5 supported on the ZrO_2 and Nb_2O_5 oxides, prepared by wet impregnation, were characterized by XRD and EPR. Their catalytic activity was tested in methanol and acetone total oxidation. Vanadium bronze samples were synthesized as a reference. Redox properties of surface oxovanadium entities were investigated by adsorption of NO probe molecule and monitored by EPR. Strong effect of the support on surface architecture of the vanadium species and their catalytic performance was observed. The highest activity in total VOC oxidation ($T_{50\%}$ = 205 °C for methanol and 230 °C for acetone) was observed for zirconia-supported catalysts containing 5.0 mol.% of V_2O_5. In all cases the niobia-supported catalysts were less active than the corresponding zirconia-supported samples.

1. Introduction

Environmentally harmful impact of volatile organic compounds (VOC) is strongly manifested by their contribution to the formation of photochemical smog, undesirable changes in troposphere composition [1,2] or possible cancerogenic effects [3,4]. Among various approaches, low-temperature catalytic oxidation belongs to the most frequently applied ways of VOC mitigation [5,6]. However, despite many studies on the total VOC oxidation, development of an efficient and economically reasonable catalyst still remains a vital problem of atmosphere protection. The reasons particularly responsible for such situation include high diversity of possible VOC compositions (halogenated and non-halogenated aliphatic and aromatic hydrocarbons, N-, O- and S-containing compounds), variety of anthropogenic emission sources (combustion, manufacture of organic chemicals, polymers and herbicides, petroleum industry, printing and painting processes [7]), as well as strong differences in reactivity exhibited by VOC mixtures in comparison to the individual components.

Several types of catalytic materials containing transition metal oxides such as V, Cr, Cu, Fe, and Mn have been tested to eliminate VOC from air [8–12], among them vanadia based catalysts belong to the most efficient and frequently used heterogeneous catalysts [13]. Catalytic activity of vanadia phase is very often enhanced by dispersion on an oxide support of high surface area (TiO_2, Al_2O_3, ZrO_2, zeolites) [14–16]. The choice of an appropriate support is a very important issue, because it can strongly modify the structure of the deposited active phase and control its distribution between the surface and the bulk. In some cases formation of new compounds *via* solid-state reaction, between the deposited phase and the support can influence the behavior of the supported catalyst.

Due to the high thermal stability and remarkable resistance to the chemical corrosion, zirconia may serve as a useful support for transition metal oxides applied in VOC removal [9,17,18]. Although niobia belongs to the less frequently used supports, it was successfully applied to form stable oxostructures of vanadium, chromium, rhenium, molybdenum and tungsten oxides, favoring the formation of two-dimensional overlayers [19–21]. Niobia is much hardly reducible than vanadia, and its hydration leads to the formation of relatively strong niobic acid, that can enhance acidic properties of the final catalyst [22].

In this work, we examine to what extent the physicochemical properties of the synthesized tetragonal ZrO_2 of enhanced thermal stability and of less stable commercial mixed-phase Nb_2O_5 supports influence the structure of the deposited VO_x entities in relation to their catalytic activity in total oxidation of methanol and acetone, chosen as representative model VOCs.

* Corresponding author.
E-mail address: adamski@chemia.uj.edu.pl (A. Adamski).

0920-5861/$ – see front matter © 2010 Elsevier B.V. All rights reserved.
doi:10.1016/j.cattod.2010.11.076

2. Experimental

Commercial niobia AHY300 support with the surface area of 177 m^2/g, calcined at 300 °C for 6 h was supplied by CBMM (Companhia Brasileira de Metalurgia e Mineração de Brazil). Reference sample of Nb_2O_5 calcined at 600 °C for 6 h has been additionally prepared. Single-phase tetragonal zirconia (S_w = 77 m^2/g) was obtained by forced hydrolysis from 0.6 M aqueous solution of $ZrOCl_2 \cdot 8H_2O$ (Aldrich 99.99%) with 25% ammonia solution at room temperature as described elsewhere in more detail [23]. The final oxide was dried at 100 °C for 24 h, and then calcined in air at 600 °C for 6 h. Supported catalysts, containing 0.5 and 5.0 mol.% of VO_x, were prepared by wet impregnation of Nb_2O_5 and *t*-ZrO_2 with an appropriate amount of aqueous solutions of ammonium metavanadate (NH_4VO_3, Merck). Wet precursors were dried in air at 100–120 °C and then calcined at 600 °C for 6 h. Additionally, highly loaded (40% VO_x) lithium-doped niobia- and zirconia-supported samples were prepared by wet impregnation together with a reference Li–V_2O_5 bronze sample. The latter one was synthesized by impregnation of the commercial vanadia (POCh) with aqueous solution of lithium nitrate to obtain 5 wt.% of Li content in the final material. The sample was next dried at 120 °C for 12 h.

X-ray diffraction patterns were recorded with X'Pert Pro (Philips, PW1710) and DRON-3 (Bourevestnik) diffractometers using monochromatized CuKα and CoKα radiations. Diffractograms were collected in the 2Θ range 20–100° with a step of 0.02–0.03°. HR-TEM images were recorded using a JEM-1000CX II UHR instrument (JEOL) operating at 100 kV. The CW-EPR X-band spectra were recorded at room (RT) and liquid nitrogen temperatures (LNT) with a Bruker ELEXSYS E-500 spectrometer operating at the 100 kHz field modulation. EPR parameters were determined by simulation using the EPRsim32 program [24]. In the model variable temperature EPR experiments the samples of the non-calcined 5VO_x/support precursors were thermally treated stepwise up to 1000 °C and every 100 °C the EPR spectrum was recorded

NO was adsorbed under the pressure of 10 Torr at LNT on the samples activated at 350–400 °C for 0.5 h in vacuum ($p \leq 10^{-5}$). The samples were next gradually exposed to room temperature or to 60 °C, to follow the adsorption progress monitored by EPR. Oxygen was introduced under the pressure of 2–5 Torr at LNT.

Catalytic tests of methanol and acetone total oxidation were performed under atmospheric pressure in a fixed-bed flow microreactor. The following composition of the gas feed was used: 0.5 vol.% of CH_3OH in the mixture containing 5 vol.% of O_2 in He (the total flow 20 cm^3/min) or 0.5 vol.% of $(CH_3)_2C{=}O$ in the mixture of the same composition (the total flow 50 cm^3/min). Catalytic test was performed in the temperature range of 100–500 °C with temperature increase of 10 °C/min. The reaction progress was measured using quadrupole mass spectrometer (PREVAC).

3. Results and discussion

3.1. Bulk structure of the carrier oxides and the supported vanadia catalysts

Both zirconia and niobia used as supports exhibit quite reach polymorphism. Depending on temperature and preparation conditions, ZrO_2 can assume a monoclinic (*m*) $P2_1/c$, a tetragonal (*t*) $P4_2/nmc$ and a cubic (*c*) $Fm3m$ form, whereas Nb_2O_5 exists in an orthorhombic (*T*), a monoclinic (*B*, *N*, *M*, *H*) and a pseudohexagonal (*TT*) variety [22,25]. The recorded XRD patterns of the bare supports were characteristic of *t*-ZrO_2 (Fig. 1a) and a mixture of *TT* and *N* (Fig. 1b) forms in the case of commercial Nb_2O_5. The crystallinity of such niobia seems to be distinctly lower than that of *t*-ZrO_2. However, the TEM microdiffraction data [26] were surprisingly more

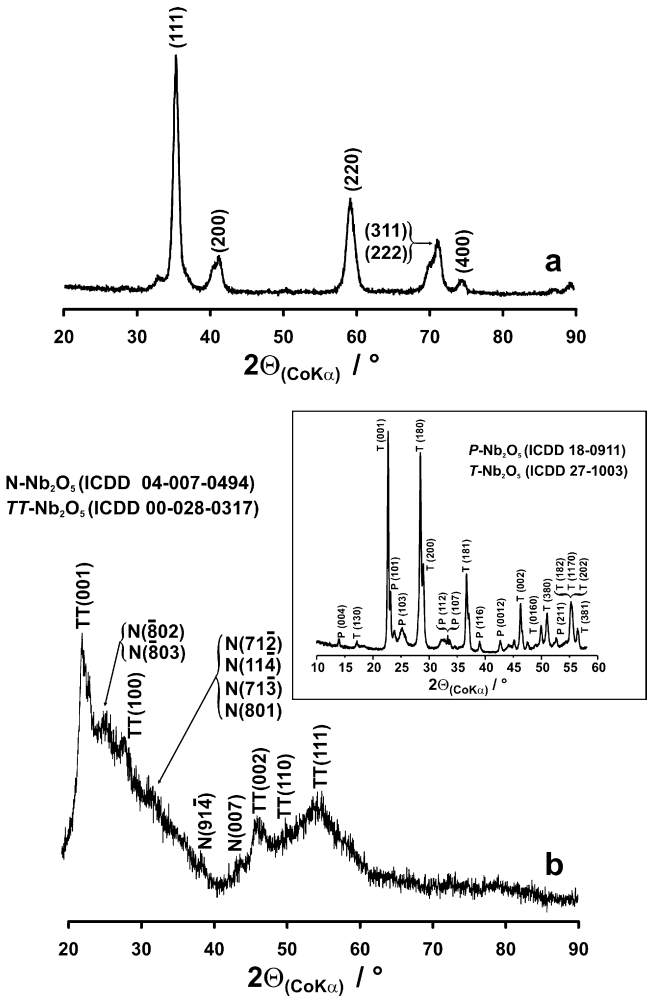

Fig. 1. XRD patterns of (a) synthesized *t*-ZrO_2 and (b) commercial Nb_2O_5 supports. In the inset, XRD pattern of the reference Nb_2O_5 calcined at 600 °C for 6 h is shown.

typical of niobia monocrystals than of polycrystalline samples. This fact can be related to the existence of well-developed crystallites of *ca.* 120 nm in size, which are separated by amorphous domains [27]. In comparison to the commercial niobia, tetragonal zirconia support exhibited higher thermal stability, remaining essentially monophasic until 600 °C, whereas Nb_2O_5 underwent progressive phase transition to thermodynamically more stable *T* and *P* forms at such conditions. Reference niobia sample, calcined at 600 °C, was fully crystalline, as it can be seen in the inset of Fig. 1. Stabilization of *t*-ZrO_2 has been related to the formation of a rigid network of nanograins, not exceeding 15 nm [28].

Impregnation of niobia and zirconia supports with ammonium metavanadate followed by subsequent calcination of both samples at 600 °C led to distinct differences in their phase composition as it can be seen in Fig. 2. Presence of 47% of the monoclinic zirconia in the 5VO_x/Zr sample was confirmed basing on the characteristic Bragg maxima at 2Θ = 26° and 33° (Fig. 2a), whereas the new compound $Nb_{23}V_2O_{62}$, formed *via* thermally-induced solid state reaction, was identified in the case of 5VO_x/Nb (Fig. 2b). Formation of $Nb_{23}V_2O_{62}$ *via* solid-state reaction of the deposited V_2O_5 with the reference Nb_2O_5 support (calcined at 600 °C) was also observed, however due to relatively low concentration of the produced $Nb_{23}V_2O_{62}$, this sample was thus excluded from further catalytic studies. No traces of segregated nanocrystalline V_2O_5 phase were found on both supports. In the case the samples containing 0.5 mol.% of VO_x only the phase transformation of the

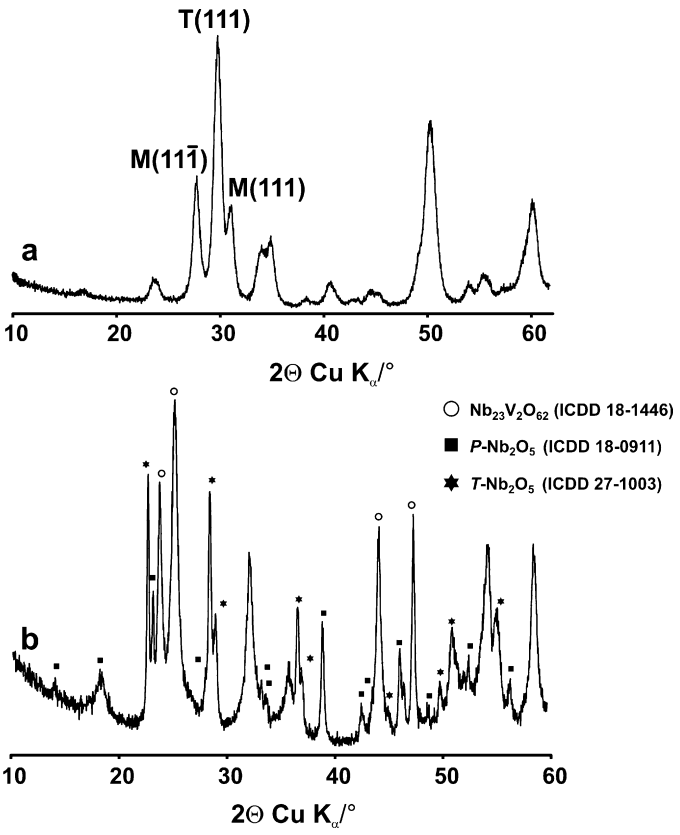

Fig. 2. XRD patterns of (a) $5VO_x$/Zr and (b) $5VO_x$/Nb catalysts calcined at 600 °C for 6 h.

zirconia and niobia supports, described above, were manifested in the corresponding XRD patterns recorded after calcination at 600 °C for 6 h.

Structure of the surface oxovanadium entities was strongly dependent on the vanadium content and the nature of the support. This effect can be associated with the differences in the point of zero charge (PZC) for both carriers. Niobia has PZC values distinctly lower (2.8) than that of ZrO_2 (6.7) [29], therefore at pH ≈ 4.0, which is typical of diluted NH_4VO_3 solutions, the surface of the niobia support is negatively charged, whereas that of zirconia – positively. As a result electrostatic repulsion of VO_3^- ions is expected to occur in the first case. Indeed, dispersion of oxovanadium species for $5VO_x$/Zr samples (gauged by the extent of magnetic interaction within the oxovanadium species) was higher than in the case of $5VO_x$/Nb, where more agglomerated species predominated at the same vanadium content. It can be clearly observed in the EPR spectra presented in Fig. 3A and B. As revealed by computer simulation, in the case of $5VO_x$/Nb catalyst, the fraction of the isolated VO_x species, giving rise to an axial signal with $g_\parallel = 1.923$ and $g_\perp = 1.976$ and a well resolved 8-line hyperfine structure due to ^{51}V nucleus ($I = 7/2$, 100%) was equal to 67%. In the case of the Nb_2O_5 carrier, the contribution of these species was below 45%. The population of polymeric species with broad ($\Delta B_{pp} = 28$ mT) and structureless EPR signal at $g_{av} = 1.96$ was equal to 22 and 57% for zirconia- and niobia-supported catalysts, respectively. In the case of samples containing 0.5 mol.% of V_2O_5 the effect of the support was less pronounced because at such low vanadium content mainly the isolated vanadyl species contributed to the EPR spectra.

The effect of temperature treatment on the structure of the surface vanadium for both supports was monitored by EPR experiments. Decay of the isolated V^{4+} surface ions with characteristic hyperfine structure, observed below 500 °C in the case of $5VO_x$/Nb sample and for $5VO_x$/Zr one above this temperature, resulted from partial oxidation of V^{4+} to V^{5+}. Subsequent changes in the spectral shape and intensity were caused by specific interaction of the VO_x entities with the niobia and zirconia supports. In the first case, the EPR spectra are characteristic of V^{4+} ions, most probably localized in the $Nb_{23}V_2O_{62}$ phase formed by solid-state reaction of both oxides. On the other hand, changes observed in the sequence of EPR spectra recorded for $5VO_x$/Zr illustrate migration of the surface vanadium ions into the bulk of the zirconia support. The final spectrum with a well-resolved hyper fine structure and $g_1 = 1.889$, $g_2 = 1.977$ and $g_3 = 1.942$, recorded after treatment of the sample at 900 °C, was characteristic of V^{4+} in the $V_xZr_{1-x}O_2$ solid solution as explained elsewhere [30]. Diffusion of vanadium ions into the matrix was

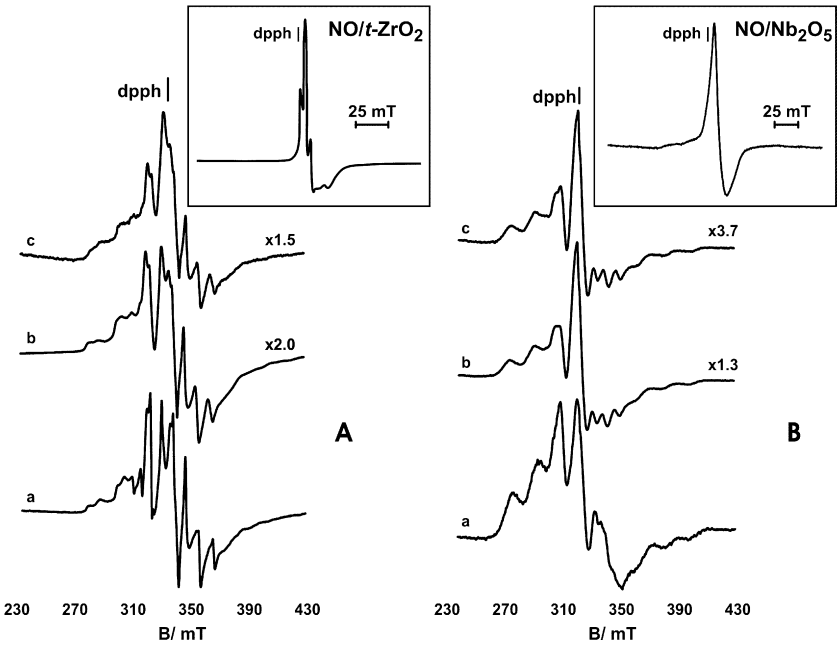

Fig. 3. EPR spectra of $5VO_x$/Zr (A) and $5VO_x$/Nb (B) catalysts before (a) and after (b) adsorption of NO ($p_{NO} = 10$ Torr) at LNT and after subsequent exposure to RT for 10 min (c). In the insets, EPR spectra of *t*-ZrO_2 and Nb_2O_5 supports after adsorption of NO ($p_{NO} = 10$ Torr) at LNT.

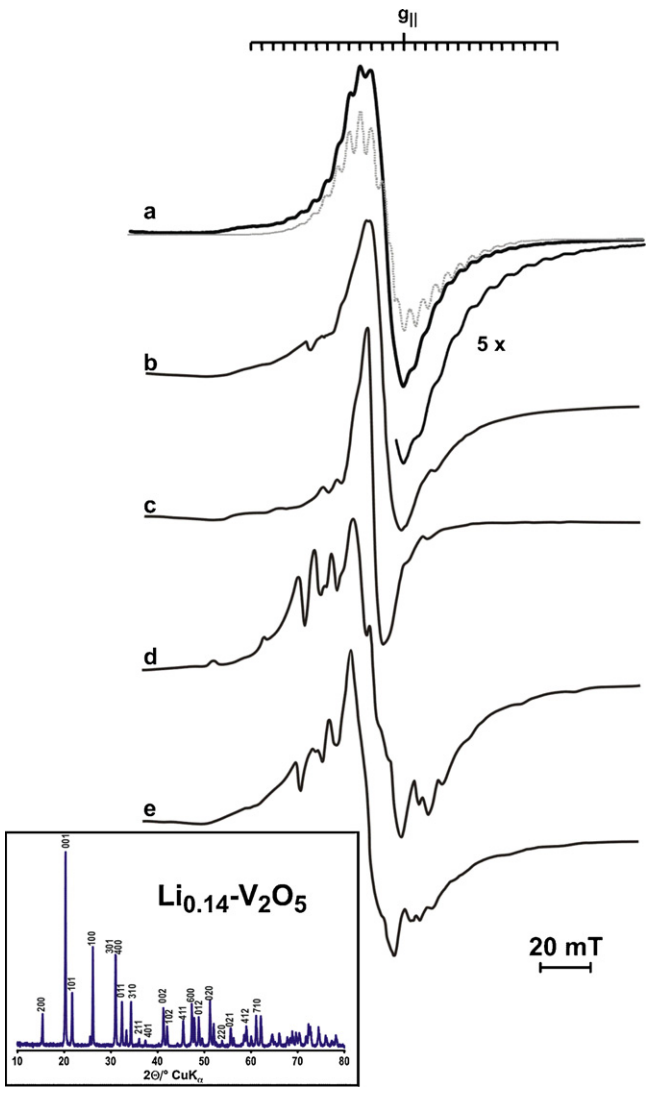

Fig. 4. EPR spectra of (a) $Li_{0.14}$–V_2O_5 (solid line) and simulated signal from vanadium bronze (dotted grey line), (b) Li–40VO_x/Zr obtained by consecutive impregnation of *t*-ZrO_2 with NH_4VO_3 solution followed by $LiNO_3$ solution, (c) Li–40VO_x/Zr obtained by simultaneous impregnation with solutions of both precursors salts, (d) Li–40VO_x/Zr obtained by consecutive impregnation of *t*-ZrO_2 with $LiNO_3$ solution followed by NH_4VO_3 solution, (e) Li–40VO_x/Nb obtained by consecutive impregnation of Nb_2O_5 with NH_4VO_3 solution followed by $LiNO_3$ solution. In the inset, XRD pattern of $Li_{0.14}$–V_2O_5 is shown.

accompanied by the tetragonal to monoclinic zirconia phase transition, strongly accelerated above 500 °C. In the case of the 5VO_x/Nb system, formation of the $Nb_{23}V_2O_{62}$ compound prevented surface depletion of vanadium.

As a reference for Li-doped highly loaded vanadia samples Li–40VO_x/support bulk $Li_{0.14}$–V_2O_5 bronze sample was also synthesized. The amount of lithium ions corresponded to α phase of vanadium bronze [31,32]. The XRD pattern of the synthesized $Li_{0.14}$–V_2O_5 sample is shown in Fig. 4 (inset), and at such a low lithium concentration it is practically the same as for the parent rhombic V_2O_5, even if the intensities of a few Bragg reflections exhibited weak deviations caused by the presence of Li^+ cations. The unpaired electrons produced by the valence pinning with Li are delocalized between the neighboring vanadium ions, which is well manifested in the low temperature axial EPR spectrum, recorded for $Li_{0.14}$–V_2O_5 sample, exhibiting characteristic 29-line hyperfine splitting at $g = 1.923$ (Fig. 4a, solid line), further confirmed by computer simulation (Fig. 4a, dotted line). Both the number of the hyperfine lines and the corresponding splitting $|A_{II}| = 4.5$ mT indicates that the unpaired electron interacts with four magnetically equivalent V centers, which is the fingerprint of the α-bronze formation [33]. Unfortunately despite numerous attempts to disperse the bronze on the zirconia and niobia surface the supported bronze catalysts were not successfully synthesized, as it can be inferred from the inspection of the corresponding EPR spectra (Fig. 4b–e). Most probably the interactions of the deposited oxovanadium entities with the surface of both supports were strong enough to exceed the lattice energy of the α-bronze, favoring good dispersion of vanadium.

3.2. Low-temperature interaction with NO

Because the g_z component of the adsorbed NO molecule is sensitive to the surface crystal field generated at the adsorption center, it can be used as a probe for investigation of the surface redox sites. The EPR spectra recorded in the temperature range from LNT to RT, after 10 min of the NO interaction ($p_{NO} = 10$ Torr) with the surface of bare *t*-ZrO_2 and Nb_2O_5 supports are shown in the insets of Fig. 3A and B. Stabilization of NO on *t*-ZrO_2 surface seems to be stronger in comparison to Nb_2O_5 as it can be inferred from the presence of the well resolved three line hyperfine structure due to coupling of the unpaired electron with the ^{14}N nucleus ($I = 1$, 99.6%). The observed signal can be attributed to $\{Zr–NO\}^1$ surface mononitrosyl complex [34]. In the case of niobia, the EPR signal was distinctly broader and the hyperfine structure was not resolved due to restricted motion of the weakly bound NO molecules. The absence of the EPR signals attributable to Zr^{3+} and Nb^{4+} ions indicated that such sites were not produced upon interaction with the adsorbed NO. In the case of Nb_2O_5 no reduction was observed, even upon heating of the sample up to 350 °C in presence of CO.

Adsorption of NO on the low loaded zirconia and niobia supported samples was carried our following the protocol described for the bare supports. However, the deposited vanadia was now easily reduced by the adsorbed NO, as it can be concluded from the progressive increase of the V^{4+} EPR signal just after NO adsorption on both zirconia and niobia-supported samples (Fig. 3A and B(a,b)). The adsorbed nitric oxide is oxidized to nitrates previously observed by IR [35], and is stored on the catalyst surface. Dynamics of the NO interaction with the 5VO_x/Zr sample during 10 min of the exposure to room temperature was more pronounced than that of 5VO_x/Nb. The integral intensity of the EPR spectrum of NO-5VO_x/Zr decreased (Fig. 3A(b and c)), due to the spin-pairing process $NO(^2\Pi) + V^{4+}(^2D) \rightarrow \eta^1$-{V–NO}. In consequence, diamagnetic mononistrosyl adducts were formed. In the case of NO–5VO_x/Nb exposure to room temperature for 10 min was not enough to accomplish first reduction step V^{5+} to V^{4+}, as it can be inferred from progressively increasing intensity of the corresponding EPR spectra (Fig. 3B(b and c)). Basing on the EPR results of NO reaction with the 5VO_x/Nb and 5VO_x/Zr catalysts one can conclude that niobia supported vanadium species are more reluctant to reduction in comparison to zirconia supported ones.

3.3. Catalytic activity

All synthesized samples were tested in total oxidation of methanol (Fig. 5). The following trend of decreasing activity was observed: 5VO_x/Zr ($T_{50\%} = 208$ °C) > Li–40VO_x/Zr ($T_{50\%} = 230$ °C) > 5VO_x/Nb ($T_{50\%} = 237$ °C) > 0.5VO_x/Zr ≈ Li–40VO_x/Nb ($T_{50\%} = 253$ and 253.5 °C) > 0.5VO_x/Nb ($T_{50\%} = 265$ °C > $Li_{0.14}$–V_2O_5 bronze ($T_{50\%} = 281$ °C). The range of $T_{50\%}$ values is typical for supported oxide catalysts tested in total oxidation of VOC [10,12]. The trends observed in methanol oxidation were confirmed also in acetone total oxidation (Fig. 5, inset). The corresponding $T_{50\%}$ temperatures differed only by 1–2 °C from those

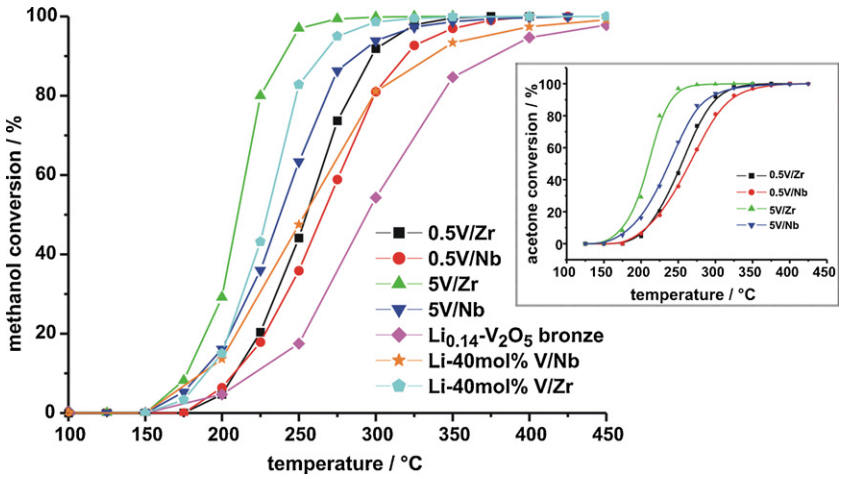

Fig. 5. Catalytic activity of investigated samples in total oxidation of methanol. In the inset, conversion of acetone for selected samples is shown.

determined for the corresponding samples tested in methanol incineration. Catalytic activity decreased in the sequence: $5VO_x/Zr$ ($T_{50\%} = 209\,^{\circ}C$) > $5VO_x/Nb$ ($T_{50\%} = 238\,^{\circ}C$) > $0.5VO_x/Zr$ ($T_{50\%} = 255\,^{\circ}C$) > $0.5VO_x/Nb$ ($T_{50\%} = 266\,^{\circ}C$). In both cases of niobia- and zirconia-supported catalysts, independently of vanadia loading, the traces of partial oxidation products were detected in temperature range of 130–380 °C. In the first step of catalytic reaction methanol was partially oxidized to formaldehyde, formic acid and dimethyl ether, whereas acetone underwent partial oxidation to acetaldehyde and acetic acid. Subsequently, all intermediates were converted into the products of total oxidation.

The catalytic activity of the zirconia-supported samples was in all cases distinctly higher at the given vanadia loading than those supported on niobia. It is also quite evident that activity in methanol incineration well corresponded to the predominant population of polymeric oxovanadium species, which can be explained by better reducibility of the two-dimensional polymeric V–O–V bridges in comparison V_2O_5 nanocrystals [36]. As implied by EPR studies, the abundance of the polymeric V–O–V species on the surface of the niobia-supported samples was even higher than in the case of the most active $5VO_x/Zr$ sample, however due to the formation of $Nb_{23}V_2O_{62}$ compound, their reducibility is distinctly weaker. In such a case vanadium is stabilized mainly as a lattice V(V) species, and cannot be easily reduced without destruction of the $Nb_{23}V_2O_{62}$ structure. Comparing the activity of the two samples supported on the same carrier but differing in vanadia loading it can noticed that the $\Delta T_{50\%}$ shift is higher in the case of the ZrO_2-supported samples (45 °C) in comparison to the Nb_2O_5-supported catalysts (28 °C). It means that zirconia-supported catalysts were more sensitive to loading effects related to surface architecture and vanadium speciation than the niobia-supported catalysts.

Total oxidation of VOC can be considered as occurring according to the two-step mechanism [10]. In the first step V(V) centers are reduced to V(IV), whereas in the second step V(IV) centers are reoxidized by O_2 from the gas phase. The ability of the catalyst to switch between both oxidation states is thus indispensable condition to make total VOC oxidation feasible. Due to the formation of a new compound such redox cycle is hampered in the case of niobia-supported catalysts. Similar situation takes place in the case of the highly loaded samples since surface segregated V_2O_5 nanocrystals are more reluctant to reduction than the polymeric species, disfavoring VOC oxidation progress.

4. Conclusions

The structure and the related properties of zirconia and niobia supports such as reducibility, chemical interaction with the deposited oxide and solid state reactivity, strongly influence their interaction with the vanadium active phase, which is reflected in their catalytic behavior in methanol and acetone incineration. Zirconia-supported samples exhibited higher activity than Nb_2O_5-supported catalysts for the same vanadium loading. The half conversion temperatures of the both investigated VOCs ($T_{50\%}^{methanol} = 205\,^{\circ}C$, $T_{50\%}^{acetone} = 230\,^{\circ}C$) were the lowest for $5VO_x/Zr$ catalyst. The ZrO_2 support favors better dispersion of the most reducible oxovanadium species, which were mainly present in weakly agglomerated forms, whereas polymeric VO_x species together with a new compound $Nb_{23}V_2O_{62}$ formation are prevailing on commercial Nb_2O_5.

Acknowledgements

Authors are grateful indeed to Mrs. Zofia Piwowarska from Faculty of Chemistry of the Jagiellonian University for her help at performing catalytic tests.

The work was financially supported by the Polish Ministry of Science and Higher Education within the international research project No. DWM/N112/COST/2008. The research was partially carried out with the equipment purchased thanks to the financial support of the European Regional Development Fund in the framework of the Polish Innovation Economy Operational Program (contract no. POIG.02.01.00-12-023/08).

References

[1] R. Atkinson, Atmos. Environ. 34 (2000) 2063.
[2] A. Mellouki, G. Le Bras, H. Sidebottom, Chem. Rev. 103 (2003) 5077.
[3] http://www.epa.gov/iaq/voc.html.
[4] J.N. Armor (Ed.), Environmental Catalysis, ACS, Washington, DC, 1994.
[5] J.J. Spivey, Ind. Eng. Chem. Res. 26 (1987) 2165.
[6] http://www.megtec.com/documents/UK_Vocsidizer.pdf.
[7] C. Gariazzo, A. Pelliccioni, P. Di Filipo, S. Sallusti, A. Cecinato, Water, Air, Soil Pollut. 167 (2005) 17.
[8] K. Everaert, J. Baeyens, J. Hazard. Mater. B 109 (2004) 113.
[9] W.B. Li, J.X. Wang, H. Gong, Catal. Today 148 (2009) 81.
[10] F. Bertinchamps, M. Treinen, P. Eloy, A.-M. Dos Santos, M.M. Mestdagh, E.M. Gaigneaux, Appl. Catal. B 70 (2007) 360.
[11] V.A. de la Peña O'Shea, M.C. Álvarez-Galván, J.L.G. Fierro, P.L. Arias, Appl. Catal. B 57 (2005) 191.
[12] R. Dziembaj, M. Molenda, L. Chmielarz, M. Drozdek, M.M. Zaitz, B. Dudek, A. Rafalska-Łasocha, Z. Piwowarska, Catal. Lett. 135 (2010) 68.
[13] B.M. Weckhuysen, D.E. Keller, Catal. Today 78 (2003) 25.
[14] G. Busca, L. Lietti, G. Ramis, F. Berti, Appl. Catal. B 18 (1998) 1.
[15] K. Bourikas, C. Fountzoula, C. Kordulis, Appl. Catal. B 52 (2004) 145.
[16] Y. Habuta, N. Narishige, K. Okumura, N. Katada, M. Niwa, Catal. Today 78 (2003) 131.
[17] M. Raciulete, P. Afanasiev, Appl. Catal. A 368 (2009) 79.

[18] F. Wyrwalski, J.-F. Lamonier, S. Siffert, L. Gengembre, A. Aboukaïs, Catal. Today 119 (2007) 332.
[19] M. Cherian, M.S. Rao, G. Deo, Catal. Today 78 (2003) 397.
[20] K.V.R. Chary, Ch.P. Kumar, A. Murali, A. Tripathi, A. Clearfield, J. Mol. Catal. A 216 (2004) 139.
[21] C. Martín, G. Solana, P. Malet, V. Rives, Catal. Today 78 (2003) 365.
[22] I. Nowak, M. Ziolek, Chem. Rev. 99 (1999) 3603.
[23] P. Jakubus, A. Adamski, M. Kurzawa, Z. Sojka, J. Therm. Anal. Calorim. 72 (2003) 299.
[24] T. Spalek, P. Pietrzyk, Z. Sojka, J. Chem. Inf. Model. 45 (2005) 18.
[25] H. Schäfer, R. Gruehn, F. Schulte, Angew. Chem. 78 (1966) 28.
[26] A. Adamski, P. Zapała, J.A.J. Rodrigues, G. Djéga-Mariadassou, Z. Sojka, submitted for publication.
[27] J. Rodrigues, A. Abou Hassan, P. Da Costa, G. Djéga-Mariadassou, Proc. Int. Annual Meeting of GDRI, Zakopane, Poland, 2007.
[28] A. Adamski, P. Jakubus, Z. Sojka, Nukleonika 51 (2006) S27.
[29] G.A. Parks, Chem. Rev. 65 (1965) 177.
[30] A. Adamski, Z. Sojka, K. Dyrek, M. Che, Solid State Ionics 117 (1999) 113.
[31] J. Galy, J. Solid State Chem. 100 (1992) 229.
[32] D.W. Murphy, P.A. Christian, F.J. DiSalvo, J.V. Waszczak, Inorg. Chem. 10 (1979) 2800.
[33] G. Sperlich, W.D. Laze, Phys. Status Solidi B 65 (1974) 625.
[34] A. Adamski, G. Djéga-Mariadassou, Z. Sojka, Catal. Today 119 (2007) 120.
[35] A. Adamski, B. Gil, Z. Sojka, Catal. Today 137 (2008) 292.
[36] S. Albrecht, G. Wendt, G. Lippold, A. Adamski, K. Dyrek, Solid State Ionics 101–103 (1997) 909.